

## Article

# MG-63 and FetMSC Cell Response on Atomic Layer Deposited TiO<sub>2</sub> Nanolayers Prepared Using Titanium Tetrachloride and Tetraisopropoxide

Denis Nazarov <sup>1,2,\*</sup>, Ilya Ezhov <sup>2</sup>, Natalia Yudintceva <sup>3</sup>, Ilya Mitrofanov <sup>2</sup>, Maxim Shevtsov <sup>3,4</sup>, Aida Rudakova <sup>1</sup> and Maxim Maximov <sup>2</sup>

<sup>1</sup> Saint Petersburg State University, Universitetskaya nab, 7/9, 199034 Saint Petersburg, Russia; aida.rudakova@spbu.ru

<sup>2</sup> Peter the Great Saint Petersburg Polytechnic University, Polytechnicheskaya, 29, 195221 Saint Petersburg, Russia; iezhov1994@gmail.com (I.E.); carlemeros@gmail.com (I.M.); maximspbstu@mail.ru (M.M.)

<sup>3</sup> Institute of Cytology of the Russian Academy of Sciences (RAS), Tikhoretsky Ave., 4, 194064 Saint Petersburg, Russia; yudintceva@mail.ru (N.Y.); shevtsov-max@mail.ru (M.S.)

<sup>4</sup> Center of Translational Cancer Research (TranslaTUM), Klinikum Rechts der Isar, Technical University Munich, Einstein Str. 25, 81675 Munich, Germany

\* Correspondence: dennazar1@yandex.ru; Tel.: +7-812-428-4033

**Citation:** Nazarov, D.; Ezhov, I.; Yudintceva, N.; Mitrofanov, I.; Shevtsov, M.; Rudakova, A.; Maximov, M. MG-63 and FetMSC Cell Response on Atomic Layer Deposited TiO<sub>2</sub> Nanolayers Prepared Using Titanium Tetrachloride and Tetraisopropoxide. *Coatings* **2022**, *12*, 668. <https://doi.org/10.3390/coatings12050668>

Academic Editor: David Schaubroeck

Received: 26 April 2022

Accepted: 10 May 2022

Published: 13 May 2022

**Publisher's Note:** MDPI stays neutral with regard to jurisdictional claims in published maps and institutional affiliations.



**Copyright:** © 2022 by the authors. Licensee MDPI, Basel, Switzerland. This article is an open access article distributed under the terms and conditions of the Creative Commons Attribution (CC BY) license (<https://creativecommons.org/licenses/by/4.0/>).

**Abstract:** Titanium oxide nanocoatings were synthesized on the surface of monocrystalline silicon and ultra-fine-grained titanium by atomic layer deposition (ALD) using titanium tetrachloride (TiCl<sub>4</sub>) and titanium tetraisopropoxide (TTIP). The morphology of the samples was studied by scanning electron microscopy (SEM) and transmission electron microscopy (TEM). The structure and composition were studied by X-ray diffraction (XRD), X-ray photoelectron spectroscopy (XPS), contact angle measurements, and energy-dispersive spectroscopy (EDS). The cytological response of osteosarcoma MG-63 and human fetal mesenchymal stem cells (FetMSCs) were studied by analyzing their morphology, viability, and alkaline phosphatase activity with and without the use of medium-induced differentiation in the osteogenic direction. A significant influence of the precursor type and ALD temperature on the crystal structure, morphology, composition, and surface free energy of TiO<sub>2</sub> nanocoatings was found. The biocompatibility of amorphous non-stoichiometric and partially crystalline stoichiometric TiO<sub>2</sub> coatings was compared. Both types of cells showed faster adhesion and improved spreading on the surface for the samples from TTIP compared to those from TiCl<sub>4</sub> at the early stages of cultivation (2 h) due to the difference in composition and higher surface free energy. No cytotoxic effect was found on both types of coatings, nor was there a noticeable difference in cell differentiation. All ALD coatings provided excellent biocompatibility and osteoconductive properties.

**Keywords:** TiO<sub>2</sub>; titania; atomic layer deposition; thin films; cell viability; cell differentiation; mesenchymal stromal cells

## 1. Introduction

Titanium oxide is commonly used in medicine in the form of thin films and coatings [1,2]. The TiO<sub>2</sub> coatings serve as an active layer for biosensors [3], protective layers that prevent the biocorrosion of medical implants [4–6] or regulate the dissolution rate of biodegradable materials [7,8]. In addition, TiO<sub>2</sub> has a bactericidal effect [9] and can be used to store and release drugs [10]. Moreover, its crystalline modifications can significantly accelerate the osseointegration of the biomaterial [6,11]. In this regard, the development and optimization of methods and techniques for obtaining titanium oxide coatings with high conformality, thickness uniformity, and purity are of particular interest to

researchers. One of the most successful and promising methods for obtaining oxide thin films is atomic layer deposition (ALD).

ALD is a thin film synthesis technology based on cyclic and self-limiting chemical reactions at the gas–solid interface, whereby reactant vapors are successively chemisorbed on the substrate surface [12,13]. The cyclic nature of ALD reactions provides precise thickness control, which is especially in demand in today's high-tech industries. Due to saturation, the surface reactions are self-limiting so the growth of coatings occurs by a layer-by-layer mechanism that allows, in addition to the possibility of precise thickness control, a conformal deposition of thin films even on complex three-dimensional and porous substrates. These features have led to both an increased interest in ALD technology in the industry and also to an increased number of fundamental studies related to the use of this film synthesis method over the past decade.

For the synthesis of TiO<sub>2</sub> nanocoatings by the ALD, a number of precursors are currently used [14,15]. The most successful ones are titanium (IV) chloride—TiCl<sub>4</sub>, tetrakis(dimethylamido) titanium (IV)—TDMAT, and titanium (IV) tetraisopropoxide—TTIP. TiCl<sub>4</sub> has a high vapor pressure, reactivity, and wide ALD temperature window. However, the use of TiCl<sub>4</sub> results in the release of hydrogen chloride as a by-product of the reactions, which leads to corrosion of the ALD equipment, as well as etching of the growing titanium oxide films [14]. TDMAT has a relatively low vapor pressure so it has to be significantly heated. At the same time, the ALD process involving amidates can also be at low temperatures (less than 100 °C) [14]. This makes TDMAT promising for thermally unstable substrates. However, coatings in this case can be contaminated with nitrogen and carbon. Titanium isopropoxide is more volatile than TDMAT. Nevertheless, due to the reversibility of the ALD exchange reactions, the growth rate of TiO<sub>2</sub> coatings using TTIP is lower than that using TDMAT. It should be noted that TTIP decomposes at temperatures above 250 °C. Despite this, TTIP has been successfully used to form high-purity TiO<sub>2</sub> coatings.

Over the past few years, only a few papers have been published on the biocompatibility of ALD titanium oxide coatings. In most cases, TiO<sub>2</sub> coatings were deposited on temperature-sensitive substrates such as polybutadiene [2], collagen [15], polyetheretherketone (PEEK) [16], chitin nanofibrous membrane [17], and polylactide (PLA) [18]. So, the TDMAT and less often the TTIP precursors with ALD temperatures lower than 100 °C were used. Coatings deposited at higher temperatures (150–300 °C) on titanium [19–21], nitinol [22], and magnesium alloy [23,24] substrates have also been studied. The *in vitro* studies revealed a positive cell response and high biocompatibility of ALD titania coatings. However, depending on the ALD conditions, the results varied greatly. For example, Yang et al. showed that TiO<sub>2</sub> coatings deposited using TDMAT and H<sub>2</sub>O at 150 °C stimulated coronary artery endothelial cells' adhesion and proliferation but the coatings deposited at 200 °C did not show such positive outcomes [23]. Liu et al. also revealed the deposition temperature effect on the adhesion and proliferation of osteoblasts and fibroblasts [21].

In this regard, the study of the effect of ALD conditions on the surface characteristics of titanium oxide and the cytological response is the most important task for the successful application of ALD technology for medical purposes. Unfortunately, the available literature on this issue does not make it possible to reliably confirm this effect due to various experimental conditions (different reagents used, various coatings' thicknesses, different cell types, and *in vitro* conditions). Clearly, detailed comparative studies are needed. In addition, there are practically no studies of cell differentiation on the ALD TiO<sub>2</sub> coatings.

In this work, we studied the influence of the type of precursor pairs (TiCl<sub>4</sub>/H<sub>2</sub>O, TTIP/H<sub>2</sub>O, TTIP/O<sub>2</sub> plasma) and synthesis temperature on the morphology, structure, composition, and wettability of the titanium oxide coatings. The resulting TiO<sub>2</sub> coatings were also characterized for early adhesion, viability, and differentiation in the osteogenic direction of osteoblast-like MG-63 and fetal mesenchymal stem cells (FetMSC). To de-

termine whether the coatings have an effect that stimulates the osteogenic differentiation of cells, studies were conducted both with and without a stimulating medium.

## 2. Materials and Methods

### 2.1. Supports Preparation

Monocrystalline silicon wafers (100) (diameters—40 mm and 100 mm) and ultra-fine-grained (UFG) titanium discs (diameter—6 mm) were used as substrates for the atomic layer deposition of TiO<sub>2</sub> films. UFG titanium rods were prepared in Nanomet, (Ufa, Russia) from Grade 4 titanium as described elsewhere [25,26]. The rods were cut into discs (thickness about 3 mm) with the Buehler IsoMet 1000 (Buehler, Lake Bluff, IL, USA) and polished by a semiautomatic Buehler MiniMet 1000 (Buehler, Lake Bluff, IL, USA) to the mirror-like surface using 200, 400, 800, and 1200 grit sandpapers and suspension of 50 nm SiO<sub>2</sub> nanoparticles. The polished titanium substrates were cleaned by successive ultrasonic treatments in acetone (99%, VEKTON, Saint Petersburg, Russia), isopropyl alcohol (99%, VEKTON, Saint Petersburg, Russia), and deionized water (resistivity 18.2 MΩ cm).

### 2.2. Atomic Layer Deposition of TiO<sub>2</sub>

Technological parameters of the ALD process, such as the reagents pulse and purge times and reactor pressures, were chosen based on the data from the literature [14] and our previous studies [20,27]. Deposition using TTIP/H<sub>2</sub>O and TiCl<sub>4</sub>/H<sub>2</sub>O reagent pairs was carried out on a Nanoserf setup (Nanoengineering, Saint Petersburg, Russia). TiCl<sub>4</sub> (99%, Merck, NJ, USA) and H<sub>2</sub>O vapors pulsed into the continuously purged and evacuated reactor (base pressure 15 mm Hg). TTIP (99.999%, Sigma Aldrich, Burlington, MA, USA) was injected into the reactor as part of a 5 vol. % solution in isooctane (99.9%, VEKTON, Saint Petersburg, Russia). The pulse times of TiCl<sub>4</sub>, TTIP, and H<sub>2</sub>O were 100, 10, and 100 ms, respectively. The time for purging the reactor with nitrogen (99.9999%) between reagent pulses was 10 s. The number of ALD cycles varied from 400 to 3000.

Deposition using TTIP and O<sub>2</sub> plasma was carried out on a Picosun R-150 setup (Picosun Oy, Espoo, Finland). The substrates were placed in the reactor and pumped out to a working pressure of 800 Pa. Synthesis was carried out at 250, 270, and 300 °C. The container with TTIP was heated to 70 °C. TTIP pulse time was 1.0 s, nitrogen purge time was 5 s, and plasma treatment time was 14 s. The number of ALD cycles varied from 500 to 1000.

### 2.3. Study of the Thickness and Morphology of TiO<sub>2</sub> Coatings

The thickness of the TiO<sub>2</sub> coatings deposited on the silicon substrates was measured by spectral ellipsometry (SE) (Ellipse 1891, CNT, Novosibirsk, Russia) using 350–1000 nm wave range and, selectively, by X-ray reflectometry (XRR) (D8 DISCOVER, Bruker, Billerica, MA, USA). The SE measurements were carried out at 9 different points over the entire surface of the substrates. XRR measurements were carried out in the range of angles from 0.3° to 5° with an increment of 0.01 using symmetric scattering geometry. The results were processed by the simplex method using LEPTOS 7.7.

For the morphology study, scanning electron microscopes Zeiss Merlin (Carl Zeiss, Oberkochen, Germany) and Tescan MIRA3 LMU (TESCAN, Brno—Kohoutovice, Czech Republic) were used at accelerating voltages of 15 and 10 kV, respectively. SE (secondary electrons) and In-lens regimes were used.

Cross-beam SEM-FIB workstation Carl Zeiss Auriga (Carl Zeiss, Oberkochen, Germany) was used for lamella preparation. Then the lamellas were studied using a Carl Zeiss Libra 200 FE transmission electron microscope (TEM). The distribution of elemental composition was collected by the methods of electron energy loss spectroscopy (EELS) in TEM mode and energy-dispersive X-ray (EDX) analysis in scanning transmission electron microscopy (STEM) mode.

#### 2.4. Study of the Structure and Composition of TiO<sub>2</sub> Coatings

The phase and elemental composition of the coatings were studied by X-ray phase analysis (D8 DISCOVER, Bruker) and X-ray photoelectron spectroscopy (Escalab 250Xi, Thermo Fisher Scientific, Waltham, MA, USA), respectively. XRD was conducted in the range of 20–80° with a step of 0.05 ° in surface-sensitive grazing incidence (GIXRD) modes. XPS spectra were measured with a Thermo Fisher Scientific Escalab 250Xi spectrometer. The samples were excited by Al K $\alpha$  (1486.7 eV) X-rays. Ar ions gun was used for surface sputtering. Survey spectra and high-resolution C1s, O1s, and Ti2p spectra were measured. The spectra were charge-compensated by setting the binding energy of the C1s carbon line to 284.8 eV.

The wetting behavior and surface free energy (SFE) were examined using a sessile drop method with a Theta Lite optical tensiometer (Biolin Scientific, Gothenburg, Sweden), as described elsewhere [28]. Two different liquids were used. Ultrapure deionized water served as a liquid with a dominant polar component of SFE (SFE<sub>p</sub> = 51.0 mN/m vs. SFE<sub>d</sub> = 21.8 mN/m), and copper stabilized diiodomethane (99%, Sigma-Aldrich) was used as a liquid with a dominant dispersive component of SFE (SFE<sub>d</sub> = 48.5 mN/m vs. SFE<sub>p</sub> = 2.3 mN/m). The average contact angles (CA value— $\Theta$ ) were measured, and the SFE values were calculated from these results according to the Owens–Wendt–Rabel–Kaelble (OWRK)/Fowkes approach [29].

#### 2.5. In Vitro Assessment of the Cellular Response

##### 2.5.1. Cell Culture

In vitro study was carried out at the Institute of Cytology of the Russian Academy of Sciences. Human osteosarcoma cell line (MG-63) (ATCC® CRL-1427TM) and human fetal mesenchymal stem cells derived from bone marrow (FetMSC) line cells were obtained from the shared research facility “Vertebrate cell culture collection” supported by the Ministry of Science and Higher Education of the Russian Federation (Agreement No. 075-15-2021-683). MG-63 and FetMSCs were maintained in a CO<sub>2</sub>-incubator (37 °C, 6% CO<sub>2</sub>) in DMEM medium (Sigma-Aldrich, Burlington, MA, USA) supplemented with 2 mM L-glutamine, 10% fetal bovine serum (FBS), and gentamicin (Gibco, Thermo Fisher Scientific, Waltham, MA, USA).

##### 2.5.2. Cell Morphology

Titanium samples were autoclaved in water steams at 121 °C and a pressure of 1.5 atmospheres. Then, the samples were placed into the wells of 4-well plates (Nunc, CIIIA). MG-63 and FetMSCs cells were seeded ( $1 \times 10^5$  in 20  $\mu$ L of DMEM/F12 nutrient medium) on the surface of the samples and incubated for 24 h in CO<sub>2</sub>. After incubation, cells were washed with Dulbecco’s Phosphate Buffer Saline (PBS) (Sigma-Aldrich, Burlington, MA, USA) and fixed in 2.5% glutaraldehyde in phosphate buffer (pH = 7.2, Sigma-Aldrich, Burlington, MA, USA). After 3 days the samples were washed in phosphate buffer and successively dehydrated in 30, 50, 70, 90, 96%, and absolute ethanol (30 min each). The final drying was carried out three times for 15 min using a Leica EM CPD300 dryer at CO<sub>2</sub> critical point. Finally, the Au coatings about 10 nm thick were deposited with a Leica EM SCD500. Evaluation of the cells’ morphology was performed using a scanning electron microscope Tescan MIRA3 LMU (TESCAN, Brno, Czech Republic).

##### 2.5.3. Cell Viability

The suspension of MG-63 and FetMSC cells was seeded into wells of a 96-well plate (Nunc, Ocala, FL, USA) at the same concentration (5000 cells/well). Two titanium samples of each type were placed into the wells and incubated in 1 mL of nutrient medium at 37 °C for 24 h. The conditioned medium (CM) was used to evaluate the cytotoxicity of the material with respect to the cells under study. Standard cell culture condition was used as a control. For each sample, cytotoxicity was assessed five times after 24 h contact using

the Vibrant MTT Cell Proliferation Assay Kit (Life Technologies, Carlsbad, CA, USA) according to the manufacturer's protocol.

#### 2.5.4. Cell Osteogenic Differentiation Assessments

For evaluation of the cell osteogenic differentiation, early marker alkaline phosphatase (ALP) was analyzed. The cell seeding was carried out in the same way as in the study of morphology. After seeding, 300  $\mu$ L of nutrient medium was added to each well to completely cover the samples' surfaces. The assessment was performed after 7 and 14 days of cell co-incubation on the samples with and without basal medium-induced cellular differentiation (StemPro Osteogenesis Differentiation Kit, ThermoFisher Scientific, Waltham, MA, USA). The medium was changed once a week. As a control, we used standard conditions for culturing cells on the surface of the culture plastic. The media were sampled and placed at  $-80$  °C for subsequent assessment of the presence of ALP using a Human Alkaline Phosphatase Assay ELISA Kit (Thermo Fisher Scientific, Waltham, MA, USA) according to the manufacturer's protocol. Optical density measurements were performed on a Thermo Scientific Varioskan LUX multimodal reader at a wavelength of 450 nm.

#### 2.5.5. Statistical Analysis

Two samples of each type were used for MTT-test and five samples for differentiation analysis. The number of repeats for both studies was five. The error bars in the figures represent the confidence interval (CI). Student's *t*-tests were used to evaluate the differences between the experimental and control groups. Credible interval of  $p < 0.05$  was considered statistically significant for all tests.

#### 2.6. Study of Mineralization

Additionally, cellular (MG-63 and FetMSCs) differentiation was determined by alkaline phosphatase and von Kossa staining after 3 weeks of cultivation on the culture plastic. For detection of alkaline phosphatase (ALP) cells were fixed with 4% paraformaldehyde and incubated for 60 min with BCIP-NBT solution (Sigma-Aldrich, Burlington, MA, USA). For assessment of mineralization, cells were fixed with methanol and incubated with a 2% solution of  $\text{AgNO}_3$  and a 2.5% solution of  $\text{Na}_2\text{S}_2\text{O}_5$ . Stained preparations were washed 3–4 times with distilled water and dried. Glasses were mounted with a mounting medium (Molecular Probes, Eugene, OR, USA). Images were obtained using an Axiovert 200 M microscope (Carl Zeiss, Munich, Germany) and a Leica DFC420C (Leica Microsystems, Wetzlar, Germany) digital camera.

To evaluate the mineralization ability of titania coatings, the samples were placed in simulated body fluid (SBF) for 10 days at 37 °C. A commercially available Dulbecco's phosphate-buffered saline (Sigma-Aldrich, Burlington, MA, USA) with pH = 7.4 was used as an SBF. After that, the samples were washed three times in deionized water and dried in an inert gas flow. The surface morphology was examined with a Zeiss Merlin electron microscope (Carl Zeiss, Oberkochen, Germany) using Oxford Instruments INCAx-act system for energy-dispersive X-ray spectroscopy (EDS).

### 3. Results

#### 3.1. Atomic Layer Deposition of $\text{TiO}_2$ Nanocoating on Silicon Substrate

##### 3.1.1. Thickness and Morphology of $\text{TiO}_2$ Nanocoatings

To measure the thickness of the deposited coatings, we used spectral ellipsometry (SE) and, selectively, X-ray reflectometry (XRR). The data on thickness, roughness, and density are given in Table 1. The SE and XRR data for the  $\text{TiCl}_4/\text{H}_2\text{O}$  and TTIP/ $\text{H}_2\text{O}$  samples differ significantly but converge well for the samples of the TTIP/ $\text{O}_2$  plasma samples. This difference can be explained by the difficulties in constructing an accurate model for rougher and better-crystallized films ( $\text{TiCl}_4/\text{H}_2\text{O}$  series). Nevertheless, the data obtained

clearly indicate a greater growth per cycle (GPC) for the  $\text{TiCl}_4/\text{H}_2\text{O}$  process (0.052–0.072 nm) than for the TTIP/ $\text{H}_2\text{O}$  (0.042–0.049 nm) and TTIP/ $\text{O}_2$  plasma (0.0186–0.0256 nm) processes. At the same time, TTIP series coatings have a significantly lower roughness than those of  $\text{TiCl}_4$ . The density values of all coatings are close to the density of the bulk phase of anatase  $\text{TiO}_2$  (3.9–4 g/cm<sup>3</sup>).

**Table 1.** Synthesis conditions and characteristics of  $\text{TiO}_2$  nanocoatings.

Precursor Pair	Sample		Number of ALD Cycles	Thickness by SE (GPC), nm	Thickness (by XRR), nm	Density, g/cm <sup>3</sup>	Roughness, nm
	Deposition Temperature, °C						
$\text{TiCl}_4/\text{H}_2\text{O}$	200 °C		500	26.0 ± 2.5 (0.0519) **	-	-	-
			1000	56.9 ± 6.8 (0.0569) *	50.9	3.92	6.89
	250 °C		500	25.8 ± 2.4 (0.0516) **	-	-	-
			1000	60.4 ± 8.2 (0.0604) *	63.5	3.91	4.67
	300 °C		500	36.0 ± 2.5 (0.0720) **	-	-	-
			1000	69.0 ± 11.4 (0.0690) *	58.2	3.87	4.07
	350 °C	1000	62.1 ± 9.6 (0.0621) *	60.4	3.92	4.06	
TTIP/ $\text{H}_2\text{O}$	200 °C		500	23.6 ± 1.8 (0.0472) **	-	-	-
	220 °C		3000	134.1 ± 0.4.6 (0.0447) **	-	-	-
	250 °C		500	21.2 ± 3.2 (0.0424) **	17.0	3.98	0.47
	250 °C		800	35.1 ± 0.9 (0.0439) **	26.9	4.06	0.21
	250 °C		1000	49.1 ± 2.9 (0.0491) **	-	-	-
TTIP/ $\text{O}_2$ plasma	250 °C		400	7.5 ± 1.0 (0.0187) **	-	-	-
	270 °C		500	12.8 ± 0.6 (0.0256) **	12.7	3.84	0.14
	300 °C		500	9.2 ± 1.1 (0.0186) **	10.4	3.98	0.44

\* The measurements are carried out on the surface of a silicon wafer with a diameter of 100 mm. \*\* The measurements are carried out on the surface of a silicon wafer with a diameter of 40 mm.

The surface morphology of coatings deposited on the monocrystalline silicon was studied using SEM. The samples' surfaces for the  $\text{TiCl}_4/\text{H}_2\text{O}$  series are characterized by the presence of a continuous layer of densely spaced grains. The size of the grains decreases from 100–200 nm to several tens of nanometers with an increase in the ALD temperature from 200 to 350 °C (Figure 1). This is in good agreement with the observation of a decrease in roughness found by XRR (Table 1). As indicated in [14], crystalline grains formed inside or on the surface of the amorphous  $\text{TiO}_2$  due to absorbing the amorphous layer as the coating grows. Therefore, it can be assumed that the higher the temperature, the more crystallization grains are formed, and the smaller the grain size that can fit on the limited surface of the substrate.

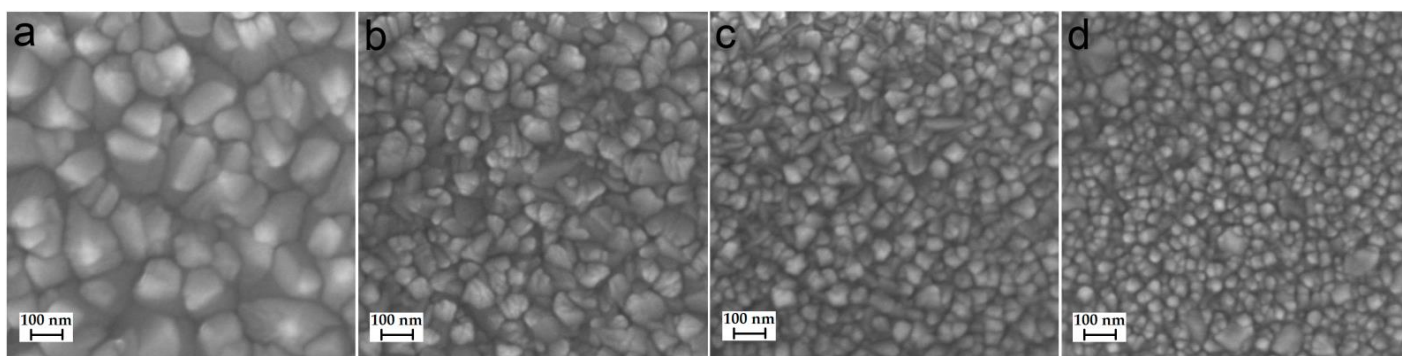


**Figure 1.** SEM images of  $\text{TiO}_2$  coatings deposited on the silicon using  $\text{TiCl}_4/\text{H}_2\text{O}$  at 200 °C (a), 250 °C (b), 300 °C (c), and 350 °C (d).

On the surface of the samples of TTIP/H<sub>2</sub>O and TTIP/O<sub>2</sub> plasma samples deposited at 250 °C, there are no significant morphological features (Figure 2a,b). Only for the TTIP/H<sub>2</sub>O samples, a faintly discernible nanotexture can be seen. However, a sample of the TTIP/O<sub>2</sub> plasma deposited at 270 °C is characterized by the presence of isolated crystalline particles ranging from several hundred nanometers to one micrometer in size (Figure 2c). For the samples obtained at 300 °C, the number of particles increases significantly; they merge and form a discontinuous layer (Figure 2d). SEM data and the XRR roughness values show that using TTIP as a precursor and ALD temperatures below 250 °C, results in uniform films with a low roughness. With an increase in the synthesis temperature, intense crystallization occurs with the formation of micron and submicron crystallites.

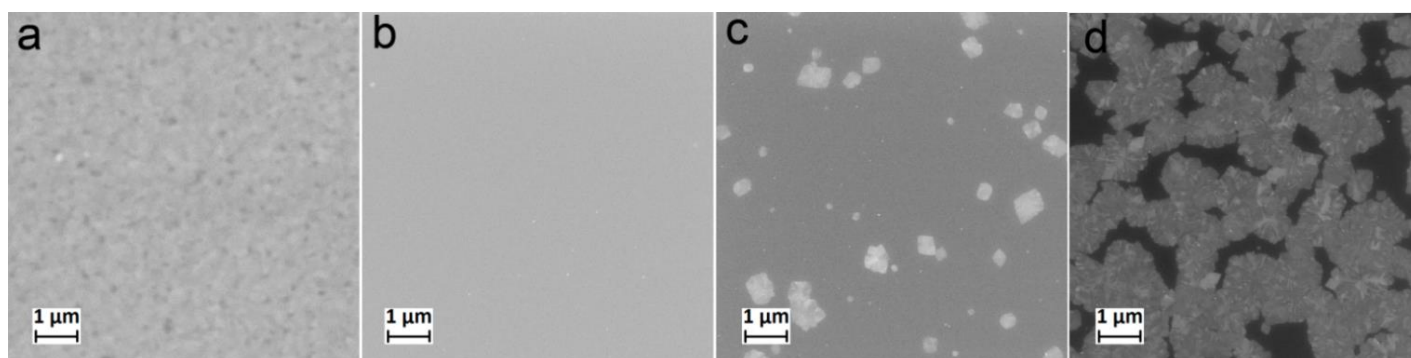


**Figure 2.** SEM images of TiO<sub>2</sub> coatings deposited on the silicon using 800 ALD cycles TTIP/H<sub>2</sub>O at 250 °C (a), 400 ALD cycles TTIP/O<sub>2</sub> plasma at 250 °C (b), 500 ALD cycles TTIP/O<sub>2</sub> plasma at 270 °C (c), and 500 ALD cycles TTIP/O<sub>2</sub> plasma at 300 °C (d).

### 3.1.2. Crystal Structure of TiO<sub>2</sub> Nanocoatings

X-ray diffraction patterns for the TiCl<sub>4</sub>/H<sub>2</sub>O samples deposited at 200, 250, 300, and 350 °C showed the presence of reflections for all samples in the region of 25, 37, 38, 39, 48, 54, 55, 63, and 75°, which corresponds to the TiO<sub>2</sub> crystal structure of anatase (Figure 3). The positions and intensities of the peaks practically do not change with an increase in the ALD temperature; however, for the sample obtained at the highest temperature (350 °C), peaks at 27.5 and 54.5° appear, which correspond to the formation of rutile TiO<sub>2</sub>.

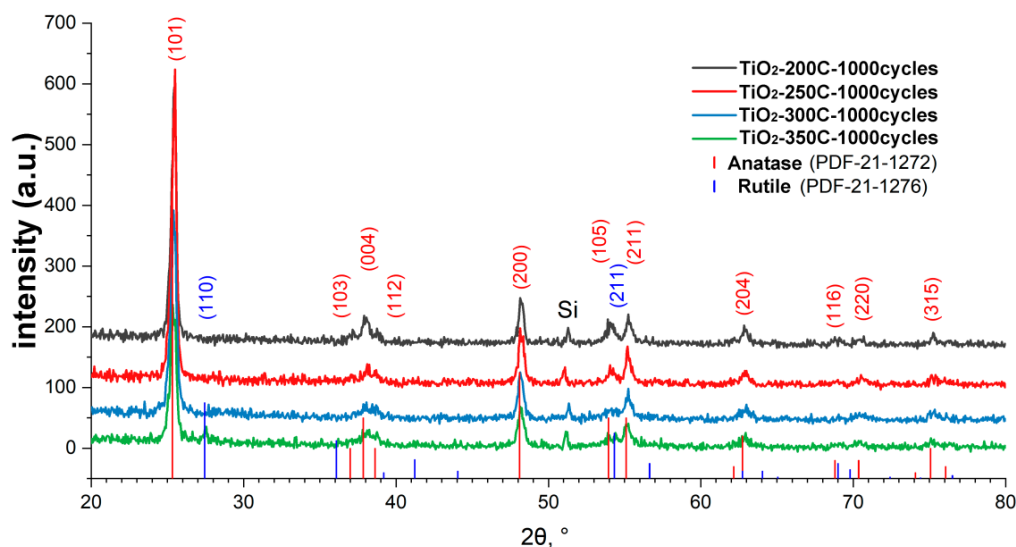


**Figure 3.** XRD patterns of titanium oxide samples obtained using TiCl<sub>4</sub> for 1000 ALD cycles on the silicon surface.

For the sample deposited using TTIP and H<sub>2</sub>O at 200 °C and 500 ALD cycles, no peaks were observed in the diffraction pattern (not shown here). Only for the sample with a large thickness of about 130 nm (3000 ALD cycles) deposited at a higher temperature—220 °C—was a small peak corresponding to the anatase TiO<sub>2</sub> observed (Figure S1). However, with the ALD temperature increasing up to 250 °C, even relatively thin films with thicknesses around 21 (500 cycles) and 35 nm (800 cycles) became polycrystalline (Figure 4). Peaks at 25, 48, 54, 55, and 63° correspond to the TiO<sub>2</sub> anatase structure. The diffraction patterns of the samples obtained using TTIP and oxygen plasma at 270 and 300 °C also contain all these peaks, except for 63°. The peaks in the region from 50 to 53° reflect the imperfection of the crystalline structure of the substrate. Despite the higher deposition temperature of the TTIP/O<sub>2</sub> plasma samples, the peak intensities are lower than those for the TTIP/H<sub>2</sub>O samples, which is probably due to the smaller film thickness.

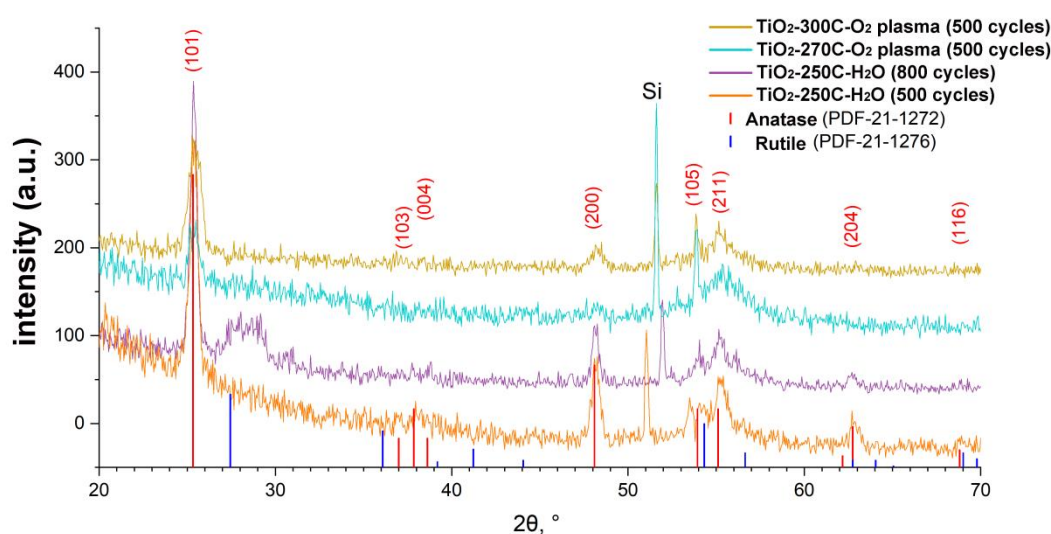


**Figure 4.** XRD patterns of titanium oxide samples deposited using TTIP on the surface of the silicon.

XRD data showed a tendency to crystallize at lower temperatures for the samples obtained using TiCl<sub>4</sub>. These results agree with the SEM data (Figures 1 and 2) and the data from the literature. In a review by Niemelä et al., it is indicated that crystallization with TiCl<sub>4</sub> can occur in the temperature range of 125–165 °C, whereas the ALD process with TTIP usually require temperatures above 200 °C [14].

### 3.2. Atomic Layer Deposition of TiO<sub>2</sub> Nanocoatings on Titanium Surface

#### 3.2.1. Thickness and Morphology of TiO<sub>2</sub> Nanocoatings

For the ALD TiO<sub>2</sub> nanocoatings on the UFG titanium, TiCl<sub>4</sub>/H<sub>2</sub>O and TTIP/H<sub>2</sub>O were used as the precursor pairs. In both cases, 200 °C and 400 ALD cycles were used. The morphology of the TiO<sub>2</sub> nanocoatings was studied by SEM. The TTIP/H<sub>2</sub>O samples do not have any surface features and the morphology of the coating is similar to the morphology of the substrate surface (Figure 5a). The surface of the TiCl<sub>4</sub>/H<sub>2</sub>O samples has a number of nanoparticles with 40–60 nm in diameter (Figure 5b,c).

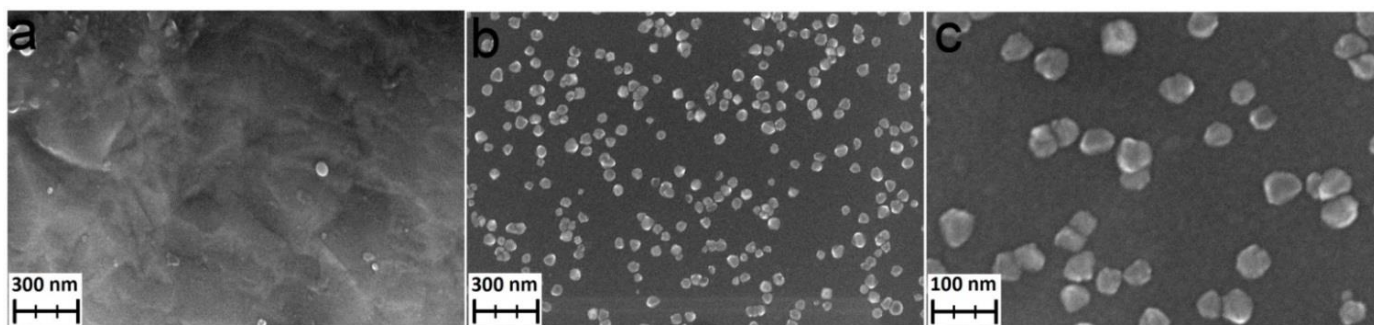


**Figure 5.** SEM images of TiO<sub>2</sub> coatings deposited on the UFG titanium using TTIP/H<sub>2</sub>O at 200 °C (a) and TiCl<sub>4</sub>/H<sub>2</sub>O at 200 °C (b,c).

According to the TEM data (Figure 6a), titanium oxide forms a continuous layer of amorphous titanium oxide with crystalline nanoparticles (Figure 5c). The thickness of the amorphous layer was about 20 nm (Figure 6b). The TEM images also clearly show an amorphous layer of native titanium oxide with a thickness of 3–4 nm, as well as an interface layer (Figure 6b) at the surface of native oxide enriched with chlorine and carbon (Figure 6c,d). The presence of carbon may be due to contamination during the polishing and storage of the titanium. The presence of chlorine can be explained by the passivation of the titanium surface by chlorine upon interaction with hydrogen chloride and hydroxychlorides formed during the ALD chemical reactions [14].

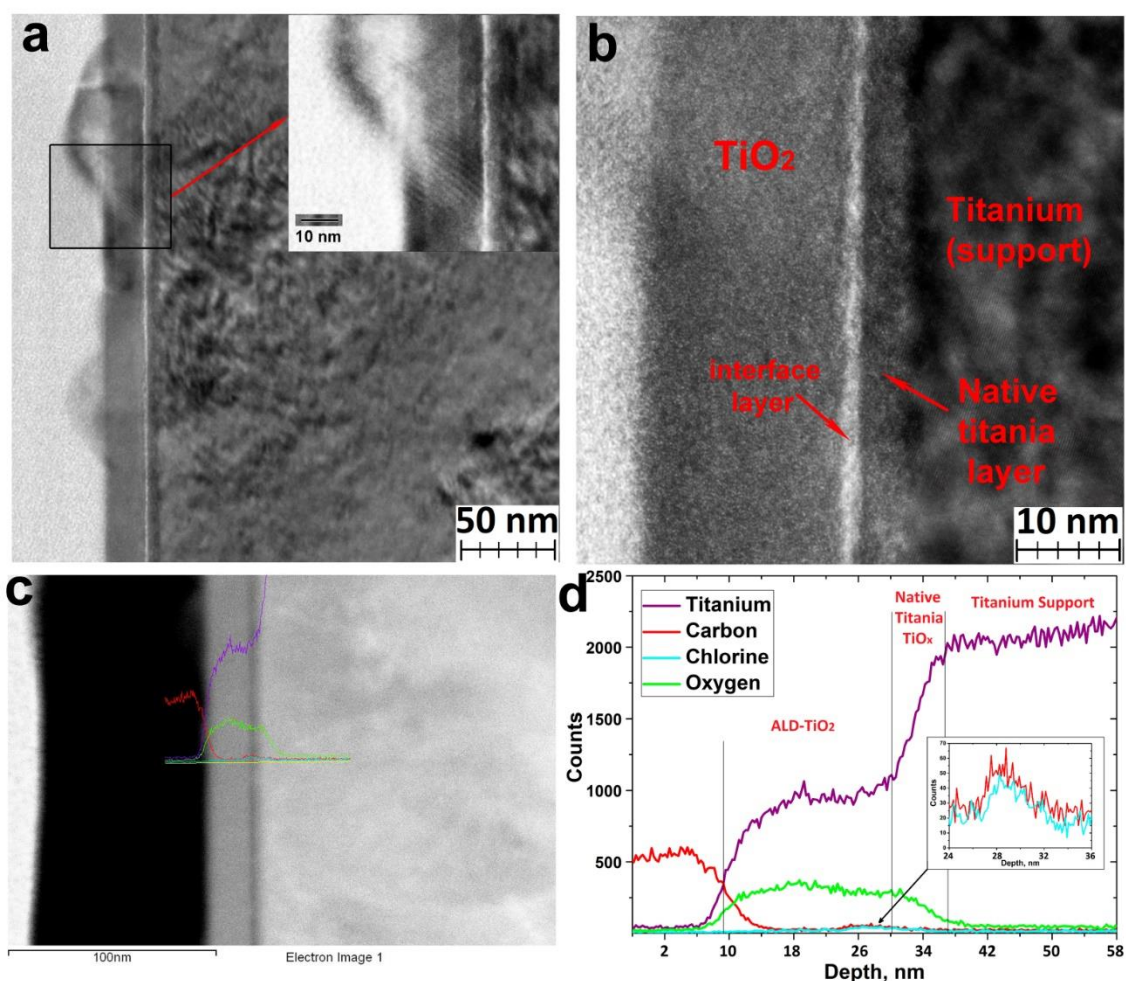


**Figure 6.** TEM images of TiO<sub>2</sub> coatings deposited on the UFG titanium using TiCl<sub>4</sub> and H<sub>2</sub>O at 200 °C (a,b), STEM images (c), and STEM-EDS profile of elemental composition (d).

### 3.2.2. Chemical Composition and Surface Free Energy of the TiO<sub>2</sub> Nanocoatings

The chemical composition of the surface and bulk of the TiCl<sub>4</sub>/H<sub>2</sub>O, TTIP/H<sub>2</sub>O, and TTIP/O<sub>2</sub> plasma coatings was studied by XPS. Titanium, oxygen, and carbon were found on the surface of all samples. Chlorine was not detected on the surface and bulk of TiCl<sub>4</sub>/H<sub>2</sub>O coatings. The C1s spectra (Figure 7a–c) for all samples show three components with maxima at 284.8, 286.2, and 288.5 eV. The most intensive peak at 284.8 eV corresponds to the aliphatic hydrocarbons (C-C, C-H) or other organic molecules but the less-intensive peak (286.2 eV) corresponds to C-OH and/or C-O groups. The smallest peaks at about 288.5 eV correspond to the carboxyl (O-C=O) and aldehyde (C=O) groups. Most of the carbon originated from surface contamination (adventitious carbon) during the storage of the samples in the air [30]. These carbon-containing compounds are exclusively concentrated on the surface of the samples and completely disappear after sputtering the surface layer with argon ions.

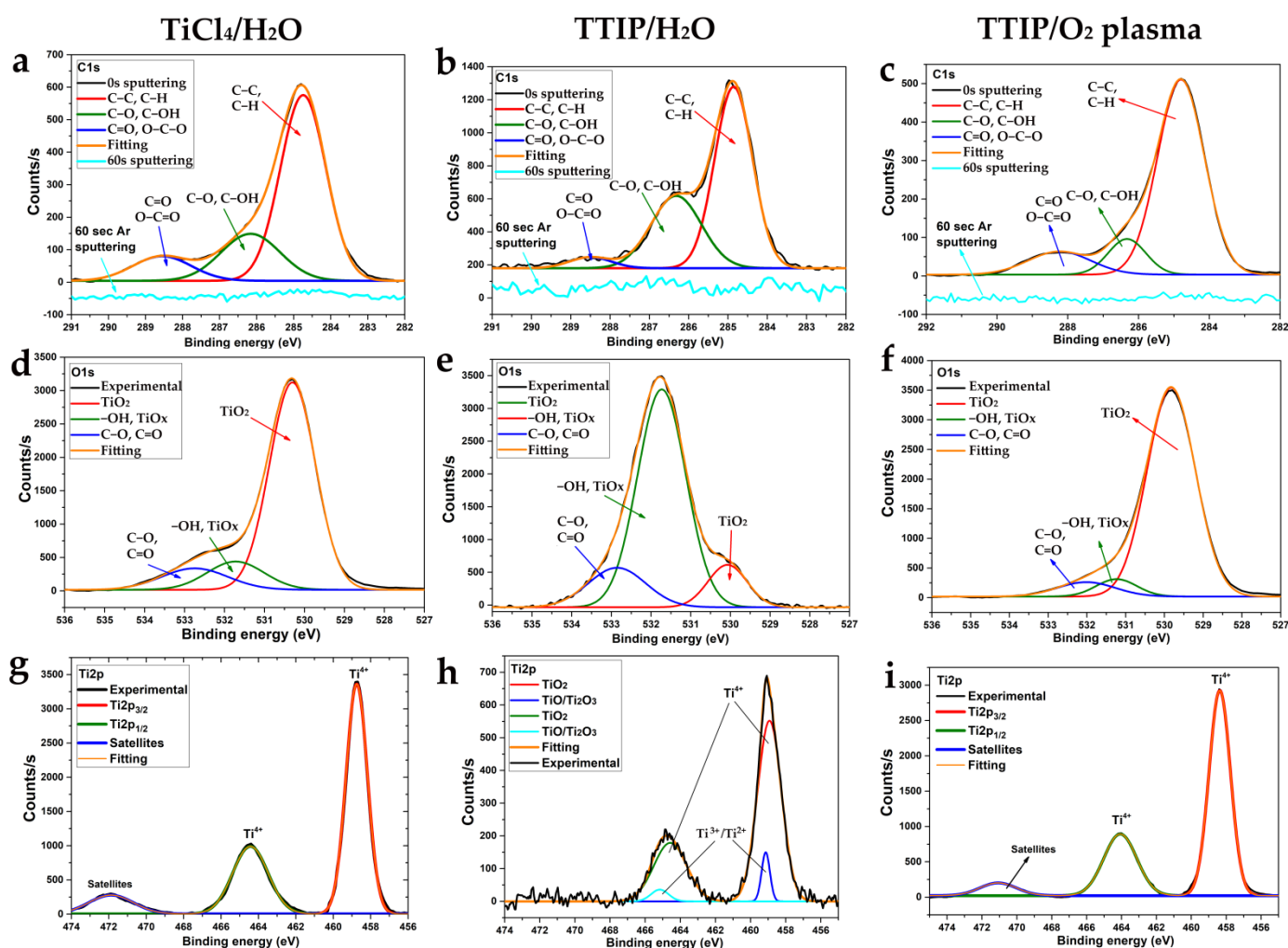


**Figure 7.** XPS C1s (a–c), O1s (d–f), and Ti2p (g–i) spectra of all studied coatings obtained using TiCl<sub>4</sub>/H<sub>2</sub>O (a,d,g), TTIP/H<sub>2</sub>O (b,e,h) and TTIP/O<sub>2</sub> plasma (c,f,i).

The O1s spectra (Figure 7d–f) of the samples show three overlapping peaks. The most intense peaks at 530.1 eV for TiCl<sub>4</sub>/H<sub>2</sub>O and TTIP/O<sub>2</sub> plasma samples belong to the oxygen of TiO<sub>2</sub>. However, for the TTIP/H<sub>2</sub>O sample, the peak at 531.2 eV is more intensive. It corresponds to both surface hydroxyl groups [31,32] and oxygen in nonstoichiometric titania (TiO<sub>x</sub>) [33]. The third peak with a maximum at 532.0 eV corresponds to the oxygen of organic surface contaminants (C-O, C=O).

The Ti2p spectra (Figure 7g–i) for all samples show intense peaks of Ti2p<sub>3/2</sub> and Ti2p<sub>1/2</sub> at 458.5–458.8 and 464.5–464.2 eV. The doublet splitting for the TiCl<sub>4</sub>/H<sub>2</sub>O and TTIP/O<sub>2</sub> plasma samples is 5.7 eV, which corresponds to TiO<sub>2</sub> [34], whereas for the TTIP/H<sub>2</sub>O sample, it is about 5.6 eV. The observed peaks for the TTIP/H<sub>2</sub>O sample are asymmetric, which is explained by the presence of the second components (peaks around 459.1 and 465.2 eV.), corresponding to titanium in lower oxidation states (Ti<sup>2+</sup>, Ti<sup>3+</sup>).

To assess the hydrophilicity and surface free energy (SFE) of the titania coatings' surface, the contact angles were measured using water and diiodomethane. Based on the obtained data, calculations of polar, dispersive, and total surface energy were carried out (Table 2). The polar component characterizes the interaction through molecular polarization forces, e.g., dipole–dipole or hydrogen bonding. The disperse component represents the interaction through nonpolar dispersion (London) forces. The polished titanium is weakly hydrophilic (the water contact angle is about 76°), whereas the value of the polar component of the SFE is smaller than that of the dispersive component. The deposition of TiO<sub>2</sub> using titanium chloride leads to a decrease in SFE due to a decrease in the polar component, and, consequently, to an increase in surface hydrophobicity (91°). The TiO<sub>2</sub> films obtained using TTIP have a weakly hydrophilic surface (74°), which is associated with a slightly higher value of its surface free energy (Table 2). In general, a clean TiO<sub>2</sub> surface like other metal oxides is a high-energy one and, therefore, should be completely wetted by most polar liquids. However, the accumulation of organic contaminants on the surface can increase the contact angle and reduce the SFE [35]. Thus, the difference in the wettability of the TiCl<sub>4</sub>/H<sub>2</sub>O and TTIP/H<sub>2</sub>O samples may be due to the differences in the composition of adsorbed to surface species, which, in turn, is associated with changes in the crystal structure, the concentration of the surface hydroxyl group, and stoichiometry of the elemental composition of the sample surface.

**Table 2.** Results of water contact angle measurements and surface free energy calculation.

Sample	Contact Angles, °	Total SFE, mN/m	Polar SFE, mN/m	Dispersive SFE, mN/m
Ti	76	37.9	7.6	30.2
TiO <sub>2</sub> (TiCl <sub>4</sub> /H <sub>2</sub> O)	91	34.0	1.6	32.4
TiO <sub>2</sub> (TTIP/H <sub>2</sub> O)	74	39.4	8.3	31.1

### 3.3. In Vitro Study of TiO<sub>2</sub> Nanocoatings on Titanium Surface

The morphology of MG-63 and FetMSCs cells after 2 and 24 h of cultivation on the polished titanium, TiCl<sub>4</sub>/H<sub>2</sub>O, and TTIP/H<sub>2</sub>O samples was studied using SEM. Good adhesion and spreading of MG-63 cells occurred for polished titanium and TTIP/H<sub>2</sub>O samples already after 2 h of cultivation (Figure 8a,c). Sample TiCl<sub>4</sub>/H<sub>2</sub>O, on the other hand, did not induce fast adhesion and spreading. The cells retained a rounded shape (Figure 8b). However, after 24 h of cultivation, the cells completely spread out on the surface of all samples. The samples coated by TiO<sub>2</sub> layers began to form outgrowths (filopodia) connecting the cells to each other (Figure 8d–f).

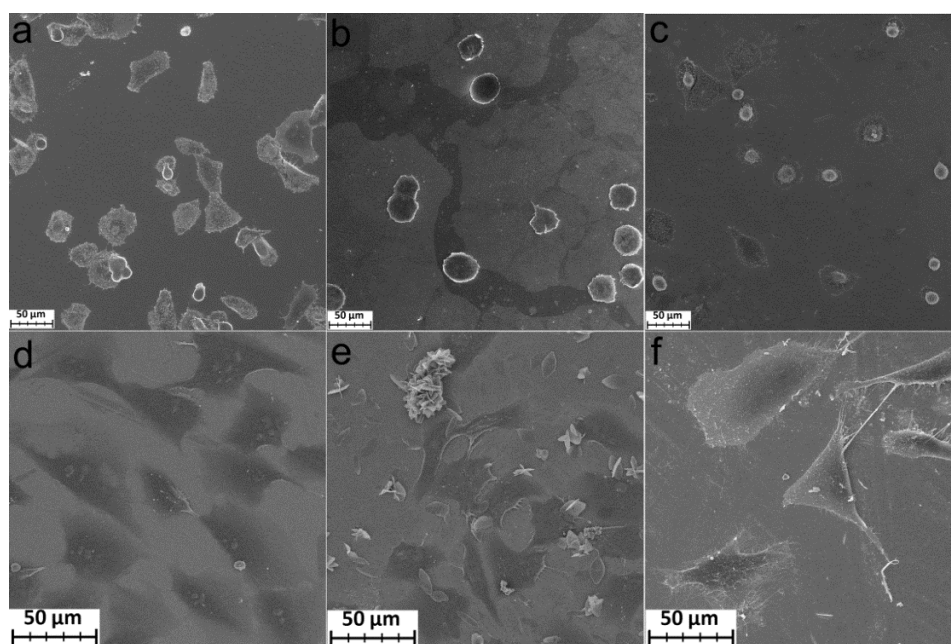


**Figure 8.** SEM images of MG-63 cells incubated during 2 h (a–c) and 24 h (d–f) on Ti (a,d), Ti-TiO<sub>2</sub> (TiCl<sub>4</sub>/H<sub>2</sub>O) (b,e), and Ti-TiO<sub>2</sub> (TTIP/H<sub>2</sub>O) (c,f) samples.

For the mesenchymal cells after 2 h of cultivation, the morphology is similar to the osteosarcoma MG-63 cells. During this period, cell spreading and adhesion began on the polished titanium and TTIP/H<sub>2</sub>O samples, but not on the TiCl<sub>4</sub>/H<sub>2</sub>O samples (Figure 9a–c). After 24 h, the cells on all samples were well-spread. The FetMSCs were elongated, bipolar, spindle-shaped (Figure 9d–f), and interconnected by filopodia (Figure S2). This morphology is typical for the cells of this line [36,37]. On the surface of TiCl<sub>4</sub>/H<sub>2</sub>O, crystalline particles with a diameter of 10–20 µm were found. These particles are evenly distributed over the surface (Figure 9f). The SEM-EDS analysis showed that they are composed of phosphorus, oxygen, and a small amount of calcium (Figure S3 and Table S1).

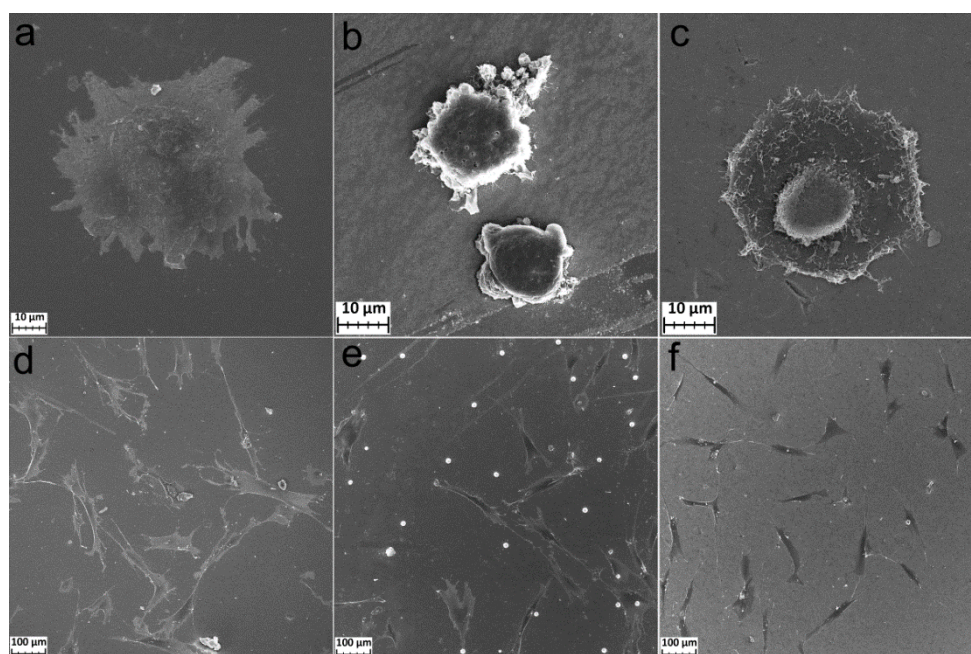


**Figure 9.** SEM images of FetMSC cells incubated during 2 h on Ti (a), Ti-TiO<sub>2</sub> (TiCl<sub>4</sub>/H<sub>2</sub>O) (b), and Ti-TiO<sub>2</sub> (TTIP/H<sub>2</sub>O) (c) samples and incubated during 24 h on Ti (d), Ti-TiO<sub>2</sub> (TiCl<sub>4</sub>/H<sub>2</sub>O) (e), and Ti-TiO<sub>2</sub> (TTIP/H<sub>2</sub>O) (f) samples.

After incubation of the MG-63 and FetMSC cells for 1 day, the cytotoxicity was measured using an MTT assay. No significant statistical difference was observed between the polished Ti, coated TiO<sub>2</sub> samples, and control samples (cells cultivated on plastic plates) for both cells (Figure S4). Since the MTT test shows the overall metabolic activity in the living cells, one can conclude that all samples did not cause toxic activity for MG-63 and FetMSC cells.

The differentiation of cells in the osteogenic direction was studied using alkaline phosphatase (ALP), which is a marker of early differentiation [38]. Studies of ALP activity were conducted with and without a special basal medium that induces cellular differentiation in the osteogenic direction. A similar trend in ALP activity change was observed for MG-63 cells on all samples using the medium (red bars) and without it (white bars) (Figure 10). The ALP activity for samples cultivated for 1 week (Figure 10a) was higher than for 2 weeks (Figure 10b). The decrease in ALP activity indicates a gradual completion of early differentiation. The induction medium had a slight positive effect in the first week of cultivation but had almost no effect in the second week for all samples, except for TiCl<sub>4</sub>/H<sub>2</sub>O. In general, the ALP activity for the TiO<sub>2</sub>-coated samples was slightly higher than for the polished titanium and significantly higher than for the control sample.

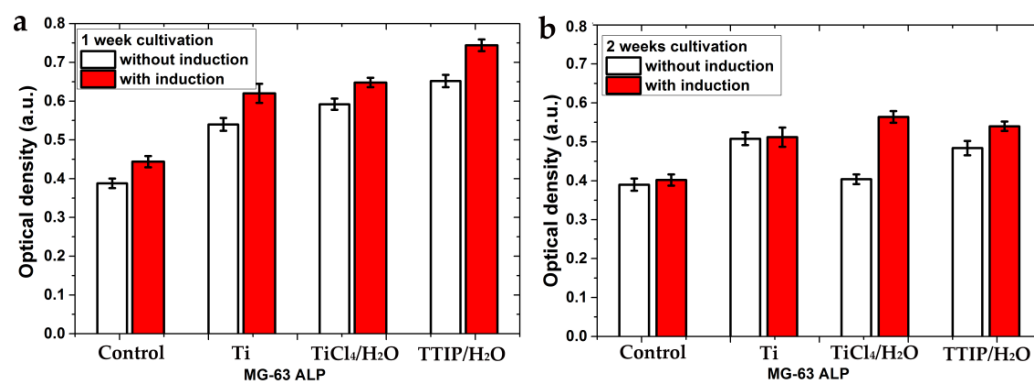


**Figure 10.** Alkaline phosphatase production by MG-63 cells on the samples with and without a medium-induced cellular differentiation in the osteogenic direction after 1 week of cultivation (a) and 2 weeks of cultivation (b). Each value represents mean  $\pm$  S.D. from five independent experiments ( $p = 0.05$ ).

The FetMSC cells showed a different trend of ALP activity than the osteoblast-like MG-63 cells. For the mesenchymal stem cells, the ALP activity increased after 2 weeks of cultivation (Figure 11). It indicates a longer process of differentiation in the osteogenic direction for these cells. A lower rate of differentiation in the osteogenic direction is an inherent characteristic of the cells of this line. Indeed, the optical photographs of the control samples (cultivation on glass slides) after 2 weeks of cultivation showed a significant difference in the differentiation of these cells (Figure 12). MG-63s represent a continuous layer of differentiated cells (Figure 12a), whereas the FetMSCs are visible as separated and partially interconnected cells (Figure 12b). For the FetMSC cells, a significant effect of the induction medium on the stimulation of osteogenic differentiation is clearly visible (Figure 11). The ALP activity for the TTIP/H<sub>2</sub>O and TiCl<sub>4</sub>/H<sub>2</sub>O samples practically do not differ from each other and slightly exceed that for the polished titanium. At the same time, all the samples show a significant superiority in differentiation compared to the control sample both with and without the induction medium.

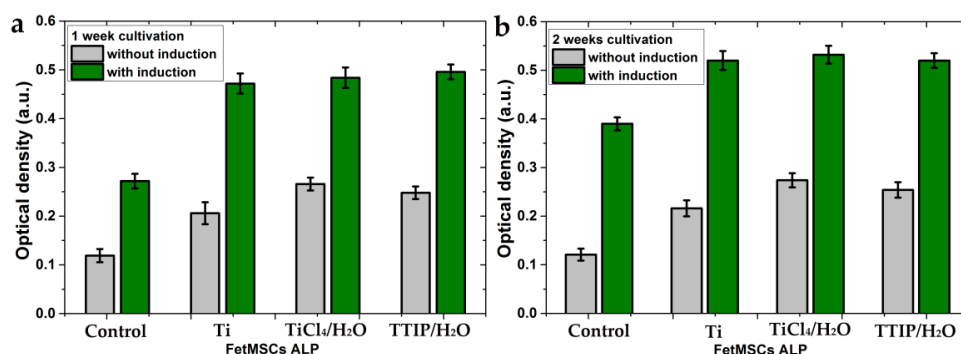


**Figure 11.** Alkaline phosphatase activity by FetMSCs on the samples with and without a medium induced cellular differentiation in the osteogenic direction after 1 week of cultivation (a) and 2 weeks of cultivation (b). Each value represents mean  $\pm$  S.D. from five independent experiments ( $p = 0.05$ ).

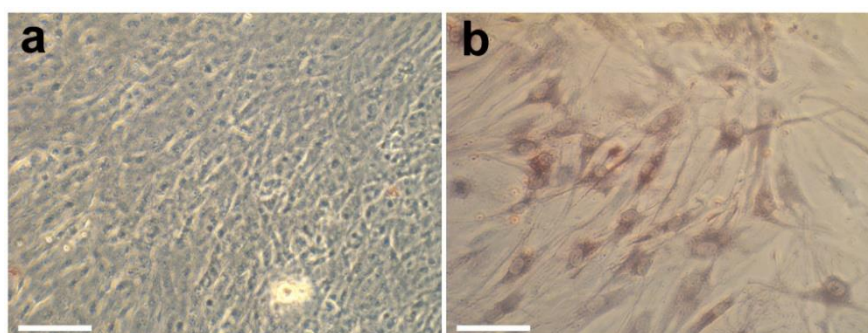


**Figure 12.** Optical microphotographs of MG-63 (a) and FetMSCs cells (b) on the surface of control samples (glass slides) after cultivation for 2 weeks. Scale bars—50  $\mu\text{m}$ .

Optical photographs of the MG-63 and FetMSC cells cultivated for 3 weeks on glass slides (control samples) using a Von Kossa stain showed that mineralization of the cells is proceeding. The beginning of mineralization is indicated by black spots corresponding to calcium phosphates (Figure S5).

When the samples were soaked in phosphate buffer for 10 days, isolated crystals tens of micrometers in size formed on their surfaces (Figure 13). These crystals are similar in morphology to crystals found earlier for the ALD-produced Ti-TiO<sub>2</sub> samples soaked in SBF for 9 days [11]. The SEM-EDS analysis showed that they are composed of phosphates with a relatively small content of calcium (Figure S6 and Table S2).

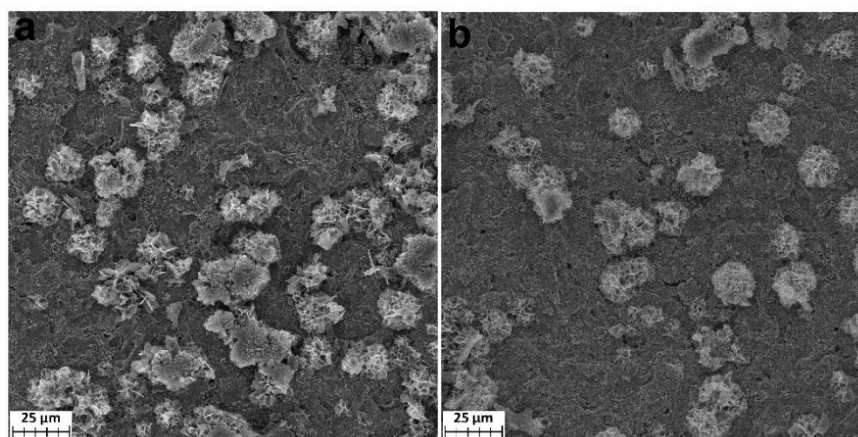


**Figure 13.** SEM images of the Ti-TiO<sub>2</sub> (TiCl<sub>4</sub>/H<sub>2</sub>O) (a) and Ti-TiO<sub>2</sub> (TTIP/H<sub>2</sub>O) (b) samples soaking in SBF for 10 days.

#### 4. Discussion

Titania nanocoatings have been successfully prepared by ALD using titanium (IV) chloride and titanium(IV) isopropoxide. It was found that the type of precursor significantly affects the crystal structure, stoichiometry, surface free energy, and wettability. This difference made it possible to synthesize coatings that differ greatly in their characteristics and cytological response. The  $\text{TiCl}_4/\text{H}_2\text{O}$  coatings have an amorphous structure with crystalline nanoparticles and stoichiometry close to  $\text{TiO}_2$ . Also, they are hydrophobic and have low surface free energy. On the contrary, the TTIP/ $\text{H}_2\text{O}$  coatings were amorphous, nonstoichiometric, hydrophilic, and have a relatively high SFE due to the polar components.

It is well-known that all the above factors should have a strong influence on the cytological response. Hydrophilicity has a positive effect on the osseointegration of the material since the most important proteins for cell adhesion and proliferation are adsorbed faster and stronger on hydrophilic surfaces [39,40]. Our results showed that at the early stages (2 h of cultivation), the osteoblast-like MG-63 and mesenchymal stem cells have poorer adhesion and spread over the more hydrophobic surface of the  $\text{TiCl}_4/\text{H}_2\text{O}$  sample. However, with a longer cultivation time (24 h), the difference practically disappears, and in terms of viability and differentiation, it is not noticeable at all. The stoichiometry (presence of  $\text{Ti}_2\text{O}_3$ ,  $\text{TiO}$ ,  $\text{Ti}_3\text{O}_5$ , etc.) and SFE are also important factors for the biocompatibility of titanium oxide coatings. However, their influence is primarily due to the effect on hydrophilicity. Indeed, Lin et al. showed that stoichiometry and the concentration of hydroxyl groups are the most important factors determining the hydrophilicity of the titanium oxide surface [41], and Vieira et al. showed that the formation of oxygen vacancies can increase in the polar component of SFE and hydrophilicity [42].

The crystal structure of  $\text{TiO}_2$  coatings is also important since various crystalline modifications and amorphous titanium oxide have different concentrations of hydroxyl groups on the surface, which determines its surface free energy and wettability [43,44]. The anatase structure is believed to be able to enhance osteoblast adhesion and proliferation by affecting wettability [45]. This difference at the initial stage is small; however, at the final stages of osseointegration, the crystal structure begins to play a more decisive role in the process of cellular mineralization. Previously, it was shown that the crystallinity of titanium oxide ALD coatings positively affects the formation of hydroxyapatite, which is one of the most important components of mature bone tissue [11]. Our results showed that ALD  $\text{TiO}_2$  coatings stimulated the formation of phosphate when samples were placed in phosphate-buffered saline. Visually, the partially crystalline  $\text{TiCl}_4/\text{H}_2\text{O}$  samples contain more phosphate crystals than the TTIP/ $\text{H}_2\text{O}$  ones; however, to confirm these findings a more detailed statistical analysis based on several samples is needed.

To date, many studies have been carried out to study the biocompatibility and cytological response of titanium oxide coatings (Table 3). Different cell lines were used but in almost all cases a positive effect of the coatings on biocompatibility has been found. The only exception is the data from the Matijošius group [46], in which ALD  $\text{TiO}_2$  showed worse biocompatibility than the much thicker magnetron sputtering coatings. The results of several other studies showed that even ultra-thin coatings (<10 nm) significantly improve the adhesion and proliferation of dental pulp stem cells [2] and the growth of fibroblasts, MG-63 osteoblasts, and human neuroblastoma [19]. At the same time, Liu showed that the coatings can simultaneously stimulate the adhesion and proliferation of preosteoblasts but impair them for fibroblasts [21]. In our study, to assess the cytological response, the most common MG-63 and less-studied FetMSC cells were used. Both cell types showed high viability and good adhesion to titania ALD nanocoatings. These results are consistent with those of most studies (Table 3).

**Table 3.** Results of in vitro study of TiO<sub>2</sub> ALD coatings using different cell lines.

Precursors, Temperature, Thickness (nm), Substrate	Crystallinity, Morphology Wettability	Cell Lines	Titanium Dioxide Effect	Ref.
TDMATi/O <sub>2</sub> plasma, 250 °C, 4–16 nm NiTi	amorphous, uniform, hydrophilic (62°)	MG-63 osteoblasts	Enhances cell adhesion, promotes cell proliferation, and reduces cytotoxicity. Increase in thickness improves positive effect	[22]
TTIP/H <sub>2</sub> O, 80 °C 3.4 nm polybutadiene	ultrathin coatings	dental pulp stem cells (DPSCs)	Improvement in adhesion and proliferation DPSCs, regulation of osteopontin and bone sialoprotein, representing osteogenic differentiation. Improved the ability to nucleate banded collagen fibers and induced the osteogenesis of DPSCs	[2]
TDAMT/O <sub>3</sub> Room temperature 150, 300, 600 cycles Collagen	water contact angle (WCA) was 0° for fresh samples, >60° after 3-day storage	osteosarcoma MG-63, human mesenchymal stem cells (hMSCs)	Improve biocompatibility promoting higher growth and proliferation of MG-63 and hMSCs, the higher level of calcium phosphate or apatite formation	[15]
TTIP/O <sub>2</sub> plasma, 100 °C 53 nm Polyetheretherketone	amorphous WCA—57° (1 day), 82° (21 days)	Mouse MSCs line ST-2.	Bioactive properties of PEEK implants are improved by TiO <sub>2</sub> thin films deposited with PEALD. Strong interaction and the focal adhesion of cells with the surface.	[16]
TTIP/H <sub>2</sub> O 70 °C 2.5–10 nm chitin nanofibrous membrane	amorphous	MC3T3-E1 preosteoblasts, NIH3T3 fibroblast	Excellent osteointegration and immunosuppressive effects and afforded well-guided bone growth by increasing affinity at the bone–chitin interfaces.	[17]
TDMAT/H <sub>2</sub> O 250 °C 5, 10 and 15 nm anodized aluminum	-	periodontal ligament stromal (PDLs)	Deposition of TiO <sub>2</sub> by ALD was less beneficial to biocompatibility than deposition by magnetron sputtering.	[46]
TiCl <sub>4</sub> /H <sub>2</sub> O 300 °C 0.28 and 8.25 nm Ti sheets and TNT *	anatase (150 cycles)	WI-38 human lung fibroblast, MG-63 osteoblasts, SH-SY5Y Human neuroblastoma	Increase in cell growth of WI-38 fibroblasts (>50%), MG-63 osteoblasts (>30%), and SH-SY5Y neuroblasts (>30%) was observed for all materials coated by five ALD cycles	[19]
TTIP/H <sub>2</sub> O 70 °C 20 nm polylactide (PLA)	-	human lung fibroblast MRC-5	High resistance to rapid degradation, biocompatible and non-toxic.	[18]
TDMAT/H <sub>2</sub> O 120, 160, 190 °C 100 nm Ti foils	190°—anatase Slightly hydrophilic, and the SFE was higher compared to the Ti control surface	human osteoblasts (PromoCell, C-12720) human dermal fibroblasts (Lonza, CC-2509)	Stimulated osteoblast adhesion and proliferation while suppressing fibroblast adhesion and proliferation compared to uncoated materials.	[21]
TDMAT/H <sub>2</sub> O 150, 200 °C 100 nm Mg-Zn alloy	WCA = 53–65°	human Coronary Artery Endothelial Cells	TiO <sub>2</sub> -150 °C stimulated cell adhesion and proliferation but TiO <sub>2</sub> -200 °C did not show positive outcomes with cell assays due to unstable surface morphology and	[23]

		less than optimal SFE		
TDMAT/H <sub>2</sub> O			TiO <sub>2</sub> + APTES **-coated AZ31 has more	
180 C	uniform and compact	mouse calvarial	favorable surface for spreading, promot-	[24]
63 nm	TiO <sub>2</sub> film	cells (MC3T3-E1)	ing viability of osteoblasts, higher ALP	
AZ31 alloy			expression	

\* TNT—titania nanotubes. \*\* APTES—(3-Aminopropyl)triethoxysilane.

There are almost no results in the literature on the effect of ALD TiO<sub>2</sub> coatings on differentiation. Chuang et al. studied the differentiation of dental pulp stem cells on the ultra-thin TiO<sub>2</sub> coatings in detail [2]. It was shown that the presence of the titania layer promotes the stabilization of extracellular matrix proteins and assists the proper folding of the collagen structure, which improves terminal differentiation. We showed that the mesenchymal cells, due to their nature, were differentiated more slowly than the osteoblast-like MG-63 cells. Also, the medium-stimulated differentiation had a markedly greater effect on the FetMSC cells. Nevertheless, both types of ALD coatings undoubtedly induce the differentiation in the osteogenic direction without the medium. Since the difference between samples TiCl<sub>4</sub>/H<sub>2</sub>O and TTIP/H<sub>2</sub>O was minimal, the influence of crystallinity and surface topography on differentiation was insignificant. It is more likely that the ALD titanium oxide surface is better suited for the adsorption of signaling biomolecules that promote rapid differentiation in the osteogenic direction [2,6].

Despite all the above, a comparison of the cytological response of the samples with and without coatings showed that the positive effect is not very great. Uncoated polished titanium also showed high biocompatibility and stimulation of cell differentiation in the osteogenic direction. Therefore, TiO<sub>2</sub> ALD coatings on the surface of titanium implants are not very promising for practical application, because the positive effect will be negligible. However, when using other materials, such as biodegradable magnesium alloys or alloys containing potentially hazardous elements, titanium oxide coatings can be very relevant [24]. In such cases, the ALD technology will be very good, because the resulting coatings have excellent uniformity, conformality, and purity. It should be emphasized that the most important advantage of ALD is the ability to deposit uniform coatings on the implant surfaces of the most diverse and complex shapes and to process a large number of implants simultaneously. Thereby, ALD is already actively used in the manufacture of dental implant coatings [8,47,48].

## 5. Conclusions

Titanium oxide nanocoatings prepared by ALD on silicon surface using TiCl<sub>4</sub> and H<sub>2</sub>O have an anatase structure even at the lowest temperature of 200 °C. At a synthesis temperature of 350 °C, in addition to anatase, a high-temperature rutile phase appears. When using TTIP, the crystallization of films begins in the range from 220 to 250 °C and leads to the formation of anatase. The SEM and XRR data also showed that the ALD temperature and the type of precursor significantly affect the film's morphology. Amorphous samples of the TTIP series have low roughness, whereas the TiCl<sub>4</sub> samples are characterized by the formation of nanocrystalline particles formed due to the crystallization of the amorphous layer. It was found that the surface of the TiCl<sub>4</sub>/H<sub>2</sub>O samples is hydrophobic and contained stoichiometric TiO<sub>2</sub>. When using TTIP and H<sub>2</sub>O, the sample surface is hydrophilic and has a non-stoichiometric elemental composition. This difference in surface characteristics has a significant effect on human osteosarcoma MG-63 and human fetal mesenchymal stem FetMSC cell line adhesion and spreading at early stages (2 h) but has almost no effect on cell viability and differentiation. Both types of coatings have a stimulating effect on cellular differentiation in the osteogenic direction for osteoblast-like and mesenchymal stem cells.

**Supplementary Materials:** The following supporting information can be downloaded at: <https://www.mdpi.com/article/10.3390/coatings12050668/s1>, Figure S1: XRD pattern of titanium

oxide deposited using TTIP and H<sub>2</sub>O at 220 °C on the silicon surface; Figure S2: SEM images of FetMSC cells incubated during 24 h (on Ti (a,d), Ti-TiO<sub>2</sub> (TiCl<sub>4</sub>/H<sub>2</sub>O) (b,e), and Ti-TiO<sub>2</sub> (TTIP/H<sub>2</sub>O) (c,f) samples. Figure S3: SEM images of particle formed on the surface of TiCl<sub>4</sub>/H<sub>2</sub>O samples after FetMSCs cultivation during 24 h (a), and SEM-EDS spectrum in point 1 (b); Table S1: Results of SEM-EDS study for particle formed on the surface of TiCl<sub>4</sub>/H<sub>2</sub>O samples after FetMSCs cultivation during 24 h; Figure S4: MG-63 and FetMSCs cells viability after co-incubation during 24 h. Data are presented as mean ± S.D. from five independent series of experiments ( $p = 0.05$ ); Figure S5: Optical microphotographs of the control samples after cultivation of MG-63 (a) and FetMSCs cells (b) during 3 weeks with Von Kossa stain. Scale bars—50 μm. Figure S6: SEM images of crystals formed on the surface of TiCl<sub>4</sub>/H<sub>2</sub>O samples after SBF soaking for 10 days (a), and SEM-EDS spectrum in point 1 (b); Table S2: Results of SEM-EDS study for particle formed on the surface of TiCl<sub>4</sub>/H<sub>2</sub>O samples after SBF soaking for 10 days.

**Author Contributions:** Conceptualization, D.N.; methodology, D.N., I.E., N.Y., A.R. and M.S.; validation, D.N., I.E. and I.M.; formal analysis, D.N. and M.S.; investigation, D.N., I.E., N.Y. and A.R.; resources, D.N., M.M. and N.Y.; data curation, D.N., and M.S.; writing—original draft preparation, D.N., N.Y. and I.M.; writing—review and editing, D.N., A.R. and M.M.; visualization, D.N.; supervision, D.N.; project administration, D.N.; funding acquisition, D.N. All authors have read and agreed to the published version of the manuscript.

**Funding:** The research was conducted under the financial support of the Russian Science Foundation grant (project No. 20-73-00067).

**Institutional Review Board Statement:** Not applicable.

**Informed Consent Statement:** Not applicable.

**Data Availability Statement:** The main data had been provided in the article and supplementary material. Any other raw/processed data required to reproduce the findings of this study are available from the corresponding author upon request.

**Acknowledgments:** This research was conducted using the equipment of the resource centers of the Research Park of the St. Petersburg State University Innovative Technologies of Composite Nanomaterials, Center for Physical Methods of Surface Investigation, Nanotechnology Interdisciplinary Center, Centre for Molecular and Cell Technologies and Nanophotonics. A.R. acknowledges financial support from Saint Petersburg State University (Pure ID 91696387). The authors are grateful to Ruslan Valiev for the provided samples of UFG titanium, Igor Kasatkin for XRD and XRR measurements, Vladimir Kalganov for SEM measurements, Denis Danilov for the TEM study, Alexandra Koroleva for XPS measurements, and Maxim Vorobiev for assistance in sample preparation for the SEM study.

**Conflicts of Interest:** The authors declare no conflict of interest.

## References

1. Jalali, F.; Oveisi, H.; Meshkini, A. Enhanced osteogenesis properties of titanium implant materials by highly uniform mesoporous thin films of hydroxyapatite and titania intermediate layer. *J. Mater. Sci. Mater. Med.* **2020**, *31*, 114. <https://doi.org/10.1007/s10856-020-06450-1>.
2. Chuang, Y.-C.; Wang, L.; Feng, K.-C.; Subramanian, A.; Chang, C.-C.; Simon, M.; Nam, C.-Y.; Rafailovich, M. The Role of Titania Surface Coating by Atomic Layer Deposition in Improving Osteogenic Differentiation and Hard Tissue Formation of Dental Pulp Stem Cells. *Adv. Eng. Mater.* **2021**, *23*, 2100097. <https://doi.org/10.1002/adem.202100097>.
3. Smietana, M.; Koba, M.; Brzozowska, E.; Krogulski, K.; Nakonieczny, J.; Wachnicki, L.; Mikulic, P.; Godlewski, M.; Bock, W.J. Label-free sensitivity of long-period gratings enhanced by atomic layer deposited TiO<sub>2</sub> nano-overlays. *Opt. Express* **2015**, *23*, 8441–8453. <https://doi.org/10.1364/OE.23.008441>.
4. Bilo, F.; Borgese, L.; Prost, J.; Rauwolf, M.; Turyanskaya, A.; Wobrauschek, P.; Kregsamer, P.; Strelci, C.; Pazzaglia, U.; Depero, L.E. Atomic layer deposition to prevent metal transfer from implants: An X-ray fluorescence study. *Appl. Surf. Sci.* **2015**, *359*, 215–220. <https://doi.org/10.1016/j.apsusc.2015.09.248>.
5. Mansoorianfar, M.; Tavosi, M.; Mozafarinia, R.; Ghasemi, A.; Doostmohammadi, A. Preparation and characterization of TiO<sub>2</sub> nanotube arrays on Ti6Al4V surface for enhancement of cell treatment. *Surf. Coat. Technol.* **2017**, *321*, 409–415. <https://doi.org/10.1016/j.surfcoat.2017.05.016>.
6. Wu, J.-M. Nanostructured TiO<sub>2</sub> layers on Ti for bone bonding. In *Bioceramics*; Osaka, A., Narayan, R., Eds.; Elsevier Ltd.: Amsterdam, The Netherlands, 2021; pp. 25–76. <https://doi.org/10.1016/C2018-0-02713-9>.

7. Peron, M.; Bin Afif, A.; Dadlani, A.L.; Berto, F.; Torgersen, J. Improving stress corrosion cracking behavior of AZ31 alloy with conformal thin titania and zirconia coatings for biomedical applications. *J. Mech. Behav. Biomed. Mater.* **2020**, *111*, 104005. <https://doi.org/10.1016/j.jmbbm.2020.104005>.
8. Hashemi Astaneh, S.; Faverani, L.P.; Sukotjo, C.; Takoudis, C.G. Atomic layer deposition on dental materials: Processing conditions and surface functionalization to improve physical, chemical, and clinical properties—A review. *Acta Biomater.* **2021**, *121*, 103–118. <https://doi.org/10.1016/j.actbio.2020.11.024>.
9. Pessoa, R.S.; dos Santos, V.P.; Cardoso, S.B.; Doria, A.C.O.C.; Figueira, F.R.; Rodrigues, B.V.M.; Testoni, G.E.; Fraga, M.A.; Marciano, F.R.; Lobo, A.O.; et al. TiO<sub>2</sub> coatings via atomic layer deposition on polyurethane and polydimethylsiloxane substrates: Properties and effects on *C. albicans* growth and inactivation process. *Appl. Surf. Sci.* **2017**, *422*, 73–84. <https://doi.org/10.1016/j.apsusc.2017.05.254>.
10. Mansoorianfar, M.; Khataee, A.; Riahi, Z.; Shahin, K.; Asadnia, M.; Razmjou, A.; Hojjati-Najafabadi, A.; Mei, C.; Orooji, Y.; Li, D. Scalable fabrication of tunable titanium nanotubes via sonoelectrochemical process for biomedical applications. *Ultrason. Sonochem.* **2020**, *64*, 104783. <https://doi.org/10.1016/j.ultsonch.2019.104783>.
11. Grigal, I.P.; Markeev, A.M.; Gudkova, S.A.; Chernikova, A.G.; Mityaev, A.S.; Alekhin, A.P. Correlation between bioactivity and structural properties of titanium dioxide coatings grown by atomic layer deposition. *Appl. Surf. Sci.* **2012**, *258*, 3415–3419. <https://doi.org/10.1016/j.apsusc.2011.11.082>.
12. Miikkulainen, V.; Leskelä, M.; Ritala, M.; Puurunen, R.L. Crystallinity of inorganic films grown by atomic layer deposition: Overview and general trends. *J. Appl. Phys.* **2013**, *113*, 021301. <https://doi.org/10.1063/1.4757907>.
13. George, S.M. Atomic Layer Deposition: An Overview. *Chem. Rev.* **2010**, *110*, 111–131. <https://doi.org/10.1021/cr900056b>.
14. Niemelä, J.-P.; Marin, G.; Karppinen, M. Titanium dioxide thin films by atomic layer deposition: A review. *Semicond. Sci. Technol.* **2017**, *32*, 093005. <https://doi.org/10.1088/1361-6641/aa78ce>.
15. Bishal, A.K.; Sukotjo, C.; Jokisaari, J.R.; Klie, R.F.; Takoudis, C.G. Enhanced Bioactivity of Collagen Fiber Functionalized with Room Temperature Atomic Layer Deposited Titania. *ACS Appl. Mater. Interfaces* **2018**, *10*, 34443–34454. <https://doi.org/10.1021/acsami.8b05857>.
16. Blendingner, F.; Seitz, D.; Ottenschlager, A.; Fleischer, M.; Bucher, V. Atomic Layer Deposition of Bioactive TiO<sub>2</sub> Thin Films on Polyetheretherketone for Orthopedic Implants. *ACS Appl. Mater. Interfaces* **2021**, *13*, 3536–3546. <https://doi.org/10.1021/acsami.0c17990>.
17. Choy, S.; Oh, D.X.; Lee, S.; Lam, D.V.; You, G.; Ahn, J.S.; Lee, S.W.; Jun, S.H.; Lee, S.M.; Hwang, D.S. Tough and Immunosuppressive Titanium-Infiltrated Exoskeleton Matrices for Long-Term Endoskeleton Repair. *ACS Appl. Mater. Interfaces* **2019**, *11*, 9786–9793. <https://doi.org/10.1021/acsami.8b21569>.
18. Nguyen, V.P.; Yoo, J.; Lee, J.Y.; Chung, J.J.; Hwang, J.H.; Jung, Y.; Lee, S.M. Enhanced Mechanical Stability and Biodegradability of Ti-Infiltrated Polylactide. *ACS Appl. Mater. Interfaces* **2020**, *12*, 43501–43512. <https://doi.org/10.1021/acsami.0c13246>.
19. Motola, M.; Capek, J.; Zazpe, R.; Bacova, J.; Hromadko, L.; Bruckova, L.; Ng, S.; Handl, J.; Spatz, Z.; Knotek, P.; et al. Thin TiO<sub>2</sub> Coatings by ALD Enhance the Cell Growth on TiO<sub>2</sub> Nanotubular and Flat Substrates. *ACS Appl. Bio Mater.* **2020**, *3*, 6447–6456. <https://doi.org/10.1021/acsabm.0c00871>.
20. Nazarov, D.V.; Smirnov, V.M.; Zemtsova, E.G.; Yuditceva, N.M.; Shevtsov, M.A.; Valiev, R.Z. Enhanced Osseointegrative Properties of Ultra-Fine-Grained Titanium Implants Modified by Chemical Etching and Atomic Layer Deposition. *ACS Biomater. Sci. Eng.* **2018**, *4*, 3268–3281. <https://doi.org/10.1021/acsbiomaterials.8b00342>.
21. Liu, L.; Bhatia, R.; Webster, T.J. Atomic layer deposition of nano-TiO<sub>2</sub> thin films with enhanced biocompatibility and antimicrobial activity for orthopedic implants. *Int. J. Nanomed.* **2017**, *12*, 8711–8723. <https://doi.org/10.2147/IJN.S148065>.
22. Abbas, A.; Hung, H.-Y.; Lin, P.-C.; Yang, K.-C.; Chen, M.-C.; Lin, H.-C.; Han, Y.-Y. Atomic layer deposited TiO<sub>2</sub> films on an equiatomic NiTi shape memory alloy for biomedical applications. *J. Alloy. Compd.* **2021**, *886*, 161282. <https://doi.org/10.1016/j.jallcom.2021.161282>.
23. Yang, F.; Chang, R.; Webster, T.J. Atomic Layer Deposition Coating of TiO<sub>2</sub> Nano-Thin Films on Magnesium-Zinc Alloys to Enhance Cytocompatibility for Bioresorbable Vascular Stents. *Int. J. Nanomed.* **2019**, *14*, 9955–9970. <https://doi.org/10.2147/IJN.S199093>.
24. Huang, L.; Su, K.; Zheng, Y.-F.; Yeung, K.W.-K.; Liu, X.-M. Construction of TiO<sub>2</sub>/silane nanofilm on AZ31 magnesium alloy for controlled degradability and enhanced biocompatibility. *Rare Met.* **2019**, *38*, 588–600. <https://doi.org/10.1007/s12598-018-1187-7>.
25. Nazarov, D.; Zemtsova, E.; Smirnov, V.; Mitrofanov, I.; Maximov, M.; Yuditceva, N.; Shevtsov, M. The Effects of Chemical Etching and Ultra-Fine Grain Structure of Titanium on MG-63 Cells Response. *Metals* **2021**, *11*, 510. <https://doi.org/10.3390/met11030510>.
26. Nazarov, D.V.; Zemtsova, E.G.; Solokhin, A.Y.; Valiev, R.Z.; Smirnov, V.M. Modification of the Surface Topography and Composition of Ultrafine and Coarse Grained Titanium by Chemical Etching. *Nanomaterials* **2017**, *7*, 15. <https://doi.org/10.3390/nano7010015>.
27. Nazarov, D.V.; Zemtsova, E.G.; Valiev, R.Z.; Smirnov, V.M. Formation of Micro- and Nanostructures on the Nanotitanium Surface by Chemical Etching and Deposition of Titania Films by Atomic Layer Deposition (ALD). *Materials* **2015**, *8*, 8366–8377. <https://doi.org/10.3390/ma8125460>.
28. Nazarov, D.; Rudakova, A.; Borisov, E.; Popovich, A. Surface Modification of Additively Manufactured Nitinol by Wet Chemical Etching. *Materials* **2021**, *14*, 7683. <https://doi.org/10.3390/ma14247683>.

29. Owens, D.K.; Wendt, R.C. Estimation of the surface free energy of polymers. *J. Appl. Polym. Sci.* **1969**, *13*, 1741–1747. <https://doi.org/10.1002/app.1969.070130815>.
30. Gengenbach, T.R.; Major, G.H.; Linford, M.R.; Easton, C.D. Practical guides for X-ray photoelectron spectroscopy (XPS): Interpreting the carbon 1s spectrum. *J. Vac. Sci. Technol. A* **2021**, *39*, 013204. <https://doi.org/10.1116/6.0000682>.
31. Yi, J.-H.; Bernard, C.; Variola, F.; Zalzal, S.F.; Wuest, J.D.; Rosei, F.; Nanci, A. Characterization of a bioactive nanotextured surface created by controlled chemical oxidation of titanium. *Surf. Sci.* **2006**, *600*, 4613–4621. <https://doi.org/10.1016/j.susc.2006.07.053>.
32. Lu, X.; Wang, Y.; Yang, X.; Zhang, Q.; Zhao, Z.; Weng, L.T.; Leng, Y. Spectroscopic analysis of titanium surface functional groups under various surface modification and their behaviors in vitro and in vivo. *J. Biomed. Mater. Res. A* **2008**, *84*, 523–534. <https://doi.org/10.1002/jbm.a.31471>.
33. Kuznetsov, M.V.; Zhuravlev, J.F.; Zhilyaev, V.A.; Gubanov, V.A. XPS study of the nitrides, oxides and oxynitrides of titanium. *J. Electron Spectrosc. Relat. Phenom.* **1992**, *58*, 1–9. [https://doi.org/10.1016/0368-2048\(92\)80001-O](https://doi.org/10.1016/0368-2048(92)80001-O).
34. Biesinger, M.C.; Lau, L.W.M.; Gerson, A.R.; Smart, R.S.C. Resolving surface chemical states in XPS analysis of first row transition metals, oxides and hydroxides: Sc, Ti, V, Cu and Zn. *Appl. Surf. Sci.* **2010**, *257*, 887–898. <https://doi.org/10.1016/j.apsusc.2010.07.086>.
35. Stevens, N.; Priest, C.I.; Sedev, R.; Ralston, J. Wettability of Photoresponsive Titanium Dioxide Surfaces. *Langmuir* **2003**, *19*, 3272–3275. <https://doi.org/10.1021/la020660c>.
36. Bhat, S.; Viswanathan, P.; Chandanala, S.; Prasanna, S.J.; Seetharam, R.N. Expansion and characterization of bone marrow derived human mesenchymal stromal cells in serum-free conditions. *Sci. Rep.* **2021**, *11*, 3403. <https://doi.org/10.1038/s41598-021-83088-1>.
37. Yudintceva, N.M.; Bogolyubova, I.O.; Muraviov, A.N.; Sheykhov, M.G.; Vinogradova, T.I.; Sokolovich, E.G.; Samusenko, I.A.; Shevtsov, M.A. Application of the allogenic mesenchymal stem cells in the therapy of the bladder tuberculosis. *J. Tissue Eng. Regen. Med.* **2018**, *12*, e1580–e1593. <https://doi.org/10.1002/term.2583>.
38. Chatakun, P.; Nunez-Toldra, R.; Diaz Lopez, E.J.; Gil-Recio, C.; Martinez-Sarra, E.; Hernandez-Alfaro, F.; Ferres-Padro, E.; Giner-Tarrida, L.; Atari, M. The effect of five proteins on stem cells used for osteoblast differentiation and proliferation: A current review of the literature. *Cell. Mol. Life Sci.* **2014**, *71*, 113–142. <https://doi.org/10.1007/s00018-013-1326-0>.
39. Stewart, C.; Akhavan, B.; Wise, S.G.; Bilek, M.M.M. A review of biomimetic surface functionalization for boneintegrating orthopedic implants: Mechanisms, current approaches, and future directions. *Prog. Mater. Sci.* **2019**, *106*, 100588. <https://doi.org/10.1016/j.pmatsci.2019.100588>.
40. Majhy, B.; Priyadarshini, P.; Sen, A.K. Effect of surface energy and roughness on cell adhesion and growth—Facile surface modification for enhanced cell culture. *RSC Adv.* **2021**, *11*, 15467–15476. <https://doi.org/10.1039/d1ra02402g>.
41. Lin, Z.; Lee, G.-H.; Liu, C.-M.; Lee, I.-S. Controls in wettability of TiO<sub>x</sub> films for biomedical applications. *Surf. Coat. Technol.* **2010**, *205*, S391–S397. <https://doi.org/10.1016/j.surfcoat.2010.08.052>.
42. Vieira, T.M.; Sagás, J.C.; Pessoa, R.S.; Fontana, L.C. Multiphase titanium suboxides films grown on glass substrate: Surface energy, wettability and morphology analysis. *Surf. Interfaces* **2020**, *20*, 100610. <https://doi.org/10.1016/j.surfin.2020.100610>.
43. Hanaor, D.A.H.; Sorrell, C.C. Review of the anatase to rutile phase transformation. *J. Mater. Sci.* **2010**, *46*, 855–874. <https://doi.org/10.1007/s10853-010-5113-0>.
44. Mansoorianfar, M.; Rahighi, R.; Hojjati-Najafabadi, A.; Mei, C.; Li, D. Amorphous/crystalline phase control of nanotubular TiO<sub>2</sub> membranes via pressure-engineered anodizing. *Mater. Des.* **2021**, *198*, 109314. <https://doi.org/10.1016/j.matdes.2020.109314>.
45. He, J.; Zhou, W.; Zhou, X.; Zhong, X.; Zhang, X.; Wan, P.; Zhu, B.; Chen, W. The anatase phase of nanotopography titania plays an important role on osteoblast cell morphology and proliferation. *J. Mater. Sci. Mater. Med.* **2008**, *19*, 3465–3472. <https://doi.org/10.1007/s10856-008-3505-3>.
46. Matijošius, T.; Pivoriūnas, A.; Čebatariūnienė, A.; Tunaitis, V.; Staišiūnas, L.; Stalnionis, G.; Ručinskienė, A.; Asadauskas, S.J. Friction reduction using Nanothin Titanium layers on anodized aluminum as potential bioceramic material. *Ceram. Int.* **2020**, *46*, 15581–15593. <https://doi.org/10.1016/j.ceramint.2020.03.105>.
47. Solovyev, A.A.; Markeev, A.M.; Tetyukhin, D.V.; Kozlov, E.N.; Molchanov, S.A. Applications of atomic layer deposition in implant dentistry. *Eur. Cells Mater.* **2014**, *27*, 17.
48. Picosun Strengthens Its Presence in the Healthcare Industries. Available online: <https://markets.businessinsider.com/news/stocks/picosun-strengthens-its-presence-in-the-healthcare-industries-1028237785> (accessed on 3 May 2022).